Differential Roles of Met10, Thr11, and Lys60 in Structural Dynamics of Human Copper Chaperone Atox1[†]

Agustina Rodriguez-Granillo[‡] and Pernilla Wittung-Stafshede*[,‡,§]

Department of Biochemistry and Cell Biology, Rice University, Houston, Texas 77251, and Department of Chemistry, Umeå University, 901 87 Umeå, Sweden

Received October 2, 2008; Revised Manuscript Received December 9, 2008

ABSTRACT: Atox1 is a human copper (Cu) chaperone with the ferredoxin-like fold that binds Cu(I) via two Cys residues in a $M_{10}X_{11}C_{12}X_{13}X_{14}C_{15}$ motif located in a solvent-exposed loop. Here, we report molecular dynamics simulations that reveal the roles of Met10, Thr11, and Lys60 in Atox1 structural dynamics. Whereas Met10 is conserved in all Atox1 homologues, Thr11 and Lys60 are exchanged for Ser and Tyr in bacteria. From simulations on apo and Cu(I) forms of Met10Ala, Thr11Ala, Lys60Ala, Thr11Ser, and Lys60Tyr variants, we have compared a range of structural and dynamic parameters such as backbone/Cu-loop dynamics, Cys solvent exposure, Cys−Cys distances, and cross-correlated motions. Surprisingly, Atox1 becomes more rigid in the absence of either Thr11 or Lys60, suggesting that these residues introduce protein flexibility. Lys60 and Thr11 also participate in electrostatic networks that stabilize the Cu-bound form and, in the apo form, determine the solvent exposure of the two Cys residues. In contrast, Met10 is buried in the hydrophobic core of Atox1, and its removal results in a dynamic protein structure. Prokaryotic residues are not good substitutes for the eukaryotic counterparts implying early divergence of Cu chaperone homologues. It appears that Atox1 residues have been conserved to ensure backbone/loop flexibility, electrostatic Cu site stabilization, and proper core packing. The discovered built-in flexibility may be directly linked to structural changes needed to form transient Atox1−Cu−target complexes in vivo.

Copper (Cu) is an essential trace metal for living organisms (*1*). Many proteins that participate in cellular respiration, antioxidant defense, neurotransmitter biosynthesis, connective-tissue biosynthesis, and pigment formation use Cu as their prosthetic, active group (*2*−*5*). However, because free Cu is toxic, cells have developed highly regulated Cu trafficking pathways. Cellular Cu homeostasis is maintained by a family of proteins called Cu chaperones, which are conserved from unicellular organisms to mammals (*6*). These small, soluble proteins, which bind Cu(I) via a two-Cys motif, guide and protect the Cu ions within the cell, delivering them to the appropriate functional targets (*5, 7*−*10*). In humans, the Cu(I) chaperone Atox1 (sometimes also called HAH1) delivers Cu to metal-binding domains (MBDs)[1] of two P_{1B}-type ATPases in the secretory pathway: the Menkes (or ATP7A) and the Wilson (or ATP7B) disease proteins (*5, 8, 11*). These proteins couple ATP hydrolysis to transport of Cu into the Golgi lumen, for metalation of cuproenzymes, such as apoceruloplasmin (*12*). Several diseases are related to an imbalance in Cu homeostasis, for example, Menkes and Wilson diseases (*13, 14*) and aceruloplasminemia (*15, 16*).

Atox1 is a 68-residue protein that, like the MBDs in ATP7A and ATP7B, has a ferredoxin-like fold with a compact $\beta\alpha\beta\beta\alpha\beta$ structure and a conserved metal binding motif ($MX_1CX_2X_3C$), located in the solvent-exposed $\beta1-\alpha1$ loop, which bind a single Cu(I) (*2, 17*) (Figure 1). Structural work has demonstrated that Cu chaperones and target MBDs from various organisms possess the same fold and coordinate Cu(I) via two solvent-exposed Cys residues in the $MX_1CX_2X_3C$ motif with a S−Cu−S linear coordination geometry (*17*−*23*). Although Met is an appropriate ligand for Cu and is part of the conserved signature motif in all organisms, it is not directly involved in metal ligation (*17, 24*). Instead, it has been proposed to act as a tether that modulates Cu binding loop structure (*17, 25*). Important differences between the eukaryotic and bacterial Cu chaperones are the amino acids at position 60 (of Atox1) and X_1 in the metal binding motif. Although distant in sequence, residue 60 is situated close to the metal binding site in the tertiary structure [within 4 Å (Figure 1)]. In eukaryotic Cu chaperones, including Atox1, this residue is an invariant Lys, which is proposed to neutralize the overall negative charge of the Cu−thiolate center in the holo form (*17, 26*). In prokaryotes, the amino acid that aligns with position 60 in Atox1 is always a Tyr (*17*). On the other hand, residue X_1 is a Thr in

[†] Support for this project was provided by the Robert A. Welch Foundation (C-1588). This work was supported in part by the Rice Computational Research Cluster funded by the National Science Foundation (NSF) (Grant CNS-0421109) and a partnership among Rice University, AMD, and Cray, and by the Shared University Grid at Rice funded by NSF (Grant EIA-0216467) and a partnership among Rice University, Sun Microsystems, and Sigma Solutions, Inc.

* To whom correspondence should be addressed. E-mail: pernilla.wittung@chem.umu.se. Phone: 46-90-7865347. Fax: 46-90-7867655.

[‡] Rice University.

[§] Umeå University.

[1] Abbreviations: MBD, metal binding domain; MD, molecular dynamics; rmsd, root-mean-square deviation; rmsf, root-mean-square fluctuation; HB, hydrogen bond.

10.1021/bi8018652 CCC: $40.75
Published on Web 01/15/2009

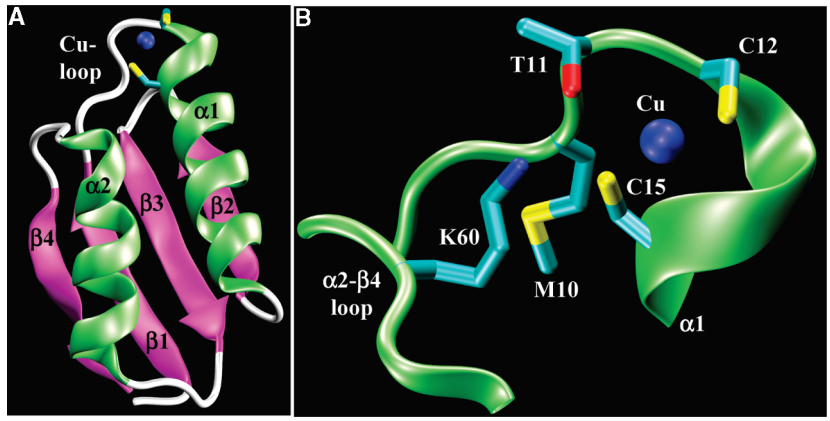

FIGURE 1: (A) Solution structure of the holo form of wild-type (WT) Atox1 (Protein Data Bank entry 1TL4) revealing its ferredoxin-like fold. The Cys (sticks) and Cu (blue) are indicated. (B) Blow-up of the Cu binding loop area. Met10, Thr11, Cys12, Cys15, Lys60, and Cu are labeled.

eukaryotic Cu chaperones, including Atox1 (Figure 1), aligning with Ser in prokaryotic Cu chaperones (*17*).

We recently reported an in vitro unfolding study of apo and holo forms of wild-type (WT) Atox1 and the bacterial homologue, *Bacillus subtilis* CopZ (*27*). We found that for both proteins, coordination of Cu stabilizes the folded state toward chemical and thermal perturbations (*27*). However, Atox1 was found to be much more resistant than CopZ to thermal perturbations. To assess the molecular origin of this in vitro difference, we performed a set of molecular dynamics (MD) simulations on WT Atox1 and CopZ with and without Cu (*24*). Our in silico MD results on apo and holo forms of Atox1 and CopZ were used to explain the in vitro findings on a molecular level (*24*).

Here we extend our computational work to address the roles of three key residues in Atox1 structural dynamics. To do this, Met10Ala, Thr11Ala, and Lys60Ala variants were generated computationally and then subjected to MD simulations in apo and Cu(I) forms. We also included Thr11Ser and Lys60Tyr variants in our study to assess how residues conserved in prokaryotic species would behave when placed in the corresponding positions in human Atox1. Surprisingly, we find that the presence of Thr11 and Lys60 destabilizes the structure of Atox1 and governs increased dynamics of the Cu binding loop. In addition, these residues are involved in a facile network of electrostatic interactions that ultimately define the Cys−Cys distance and cause negative cross correlation in the active site of the apo form. In contrast, the presence of Met10 stabilizes the core of the protein; in its absence, the protein is unstable and the Cys−Cys distance increases dramatically. The prokaryotic residues tested at positions 11 and 60 are not well-tolerated in Atox1, suggesting early divergence among Cu chaperone homologues.

COMPUTATIONAL METHODS

Protein structures were obtained from the Protein Data Bank, entries 1TL5 (*28*) and 1TL4 (*28*) for apo- and holo-Atox1, respectively. The following mutations were generated in Atox1 in silico with the *leap* module of Amber9 (*29*−*32*): Met10Ala, Thr11Ala, Thr11Ser, Lys60Ala, and Lys60Tyr. MD simulations were performed for the different protein variants using Amber9 (*29*−*32*). The initial structures were immersed in a pre-equilibrated truncated octahedral cell of TIP3P explicit water molecules (*33*), and Na^+ ions were added to neutralize the systems (*29*−*32*). Protein atoms were described with the parm99SB force field parametrization (*34*). Parameters of the coordinating Cys and Cu in the holo forms were taken from ref *24*. Briefly, the geometry of holo-Atox1 was optimized at the QM(PBE/DZP)-MM(Amber99) level (Cu with two cysteinates) followed by HF/6-31G(d)/RESP charge parametrization as described in the Amber standard protocol. Water molecules extended at least 9 Å from the surface of the proteins. Simulations were performed in the NPT ensemble [constant pressure of 1 atm and temperature of 300 K was maintained using the Berendsen coupling scheme (*35*)], employing periodic boundary conditions. A SHAKE algorithm was employed to keep bonds involving hydrogen atoms at their equilibrium length (*36*). The optimized systems were heated to 300 K and equilibrated for 200 ps. The structures were simulated until the root-mean-square deviation (rmsd) as a function of time was stable for the last 20 ns. The converged last 20 ns was used for data analysis. Rmsd, rms fluctuations (rmsf) per residue, protein/solvent radial distribution functions $g(r)$, and the cross correlation matrix of the fluctuations of the Cα atoms from their average values were calculated for each of the systems using the *ptraj* module of Amber9 (*29*−*32*).

RESULTS AND DISCUSSION

Analysis of WT Atox1. (i) Cross Correlation Analysis. In our earlier work, we performed ~22 ns MD simulations of WT apo- and holo-Atox1 and found that both forms were equilibrated in the last 20 ns (*24*). To gain insight into the effect of Cu on the cooperative dynamics of Atox1 structure, the cross correlation matrix (*37, 38*) for the Cα atoms was now calculated for apo- and holo-Atox1 (Figure 2). In this analysis, positive or in-phase correlations are colored red (strong) and yellow (moderate) and negative or out-of-phase correlations are colored cyan (moderate). We find no strong cross-correlated regions, except for the diagonal that corresponds to the correlation of a residue with itself. This is consistent with no major conformational changes occurring during the MD simulation (*24*).

In apo-Atox1, moderate positive correlation is observed between residues forming secondary structure elements, such as helices α1 and α2 and strands β1 and β3, β2 and β3, and β1 and β4, which hold the fold together. Interestingly, there are three distinct areas of negative cross correlation that are

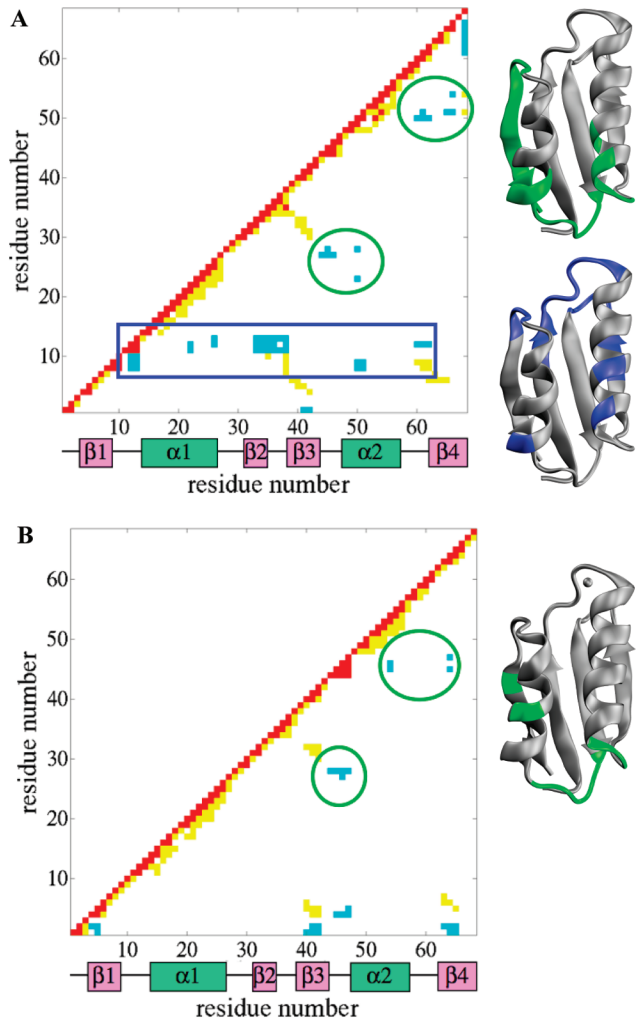

FIGURE 2: Cross correlation matrices of fluctuations of Cα atoms from their average values during the last 20 ns of the simulation for apo (A) and holo (B) forms of WT Atox1: red, strong positive correlation ($0.6 \leq C_{ij} \leq 1$); yellow, moderate positive correlation ($0.4 \leq C_{ij} < 0.6$); cyan, moderate negative correlation ($0.4 \leq |C_{ij}| < 0.6$); white, weak or no correlation ($-0.4 < C_{ij} < 0.4$). Analysis is based on previously published simulation data (*24*). Negative cross correlation regions (blue square and green circles) are mapped in the corresponding apo and holo structures with the corresponding color (insets).

indicated by a blue rectangle and two green circles (Figure 2A). The blue rectangle represents out-of-phase movements of residues located in the Cu binding loop and its vicinity, and with residues that are distant in both sequence and space. These residues are graphically highlighted in the apo structure (Figure 2A, inset). In particular, Cys12, which is the first Cys believed to bind Cu (*39*), has large (in magnitude) anticorrelation coefficients with most residues of the blue region: residues 8−10 (Cu loop, including the conserved Met10), 22 (helix α1), 26 (α1−β2 loop), 33−38 (strand β2 and β2−β3 loop), and 60−62 (α2−β4 loop, including the conserved Lys60). Also, although weakly, both Cu-coordinating Cys residues are anticorrelated with each other. The observed flexibility of the Cu loop in apo-Atox1 (*24*) may allow for these concerted out-of-phase movements and interactions between the loop and distant parts of the protein. This distinct anticorrelation pattern of the Cu loop may be important for Cu binding, possibly by positioning Cys12 in an appropriate conformation for Cu uptake. In addition, the green circles represent anticorrelated motions of residues that are mostly located at the opposite side of the Cu loop in the protein structure (Figure 2A, inset). We previously suggested that this region, in particular the β3−α2 loop, may serve as an interface for protein−protein interactions (*24*). Thus, it seems that whereas positive correlations hold the fold together, anticorrelations are predominant in regions with functional relevance. This is in agreement with previous simulations, in which regions with negative cross correlation corresponded to a protein's active site (*40*).

In holo-Atox1, the in-phase movements are similar to those found in the apo form, as expected since the fold is not greatly altered by the presence of Cu (Figure 2B). However, in sharp contrast to the apo form, the Cu loop not only loses its negative cross correlated motions with the rest of the protein (the blue region disappears) but also gains positive cross correlation with residues in helix α1. In particular, Cys12 and Cys15 now present significant in-phase motions, which is expected since both are bound to the Cu atom. Even though some of the correlations from the green regions are lost, there are still significant out-of-phase motions in these regions (particularly in the β3−α2 loop), suggesting that these concerted movements of the holoprotein may be important for subsequent Cu release, for example, by facilitating specific partner recognition during Cu transfer. Overall, this analysis supports the finding that the structural and dynamic changes occurring upon Cu binding affect mainly the Cu loop, and to a lesser extent the β3−α2 loop.

(ii) Specific Analysis of Conserved Residues. Our previous analysis (*24*) focused on residues Met10, Cys12, and Cys15, which are part of the Cu-binding motif ($MX_1CX_2X_3C$). For Met10, we found that in Atox1 this residue is always buried regardless of the presence of Cu and interacts extensively with the protein core (*24*). The interacting residues include the side chains of Ile33, Leu35, and Val40 and the backbone of Asp34, Lys38, and Lys39, all located in the β2−β3 sheet, as well as with the Cys15 side chain. Here, we extend the analysis of the WT simulation data to include residues X_1 (Thr11) and Lys60 in Atox1.

Thr11, located in the Cu loop (Figure 1), is conserved in eukaryotic Cu chaperones and MBDs (except in MBD3 where it is a His) and in prokaryotic MBDs (*17*). However, in prokaryotic Cu chaperones, this position is occupied by a Ser (*17*). In eukaryotic Cu chaperones, Thr11 is proposed to hydrogen bond (HB) with Cys12 of the partner MBD during Cu transfer (*26*). In the absence of Cu, Thr11 in Atox1 is floppy and solvent-exposed and does not interact with Cys12 or Lys60 (Figure 3A,B). On the other hand, in holo-Atox1, Thr11 is still exposed to solvent but its flexibility is significantly reduced (Figure 4C,D) and now forms a stable electrostatic interaction with Cys12 (Figure 3A). Interaction between Thr11 and Cys12 in holo-Atox1 is possible because of a strong and stable HB found between Thr11 and Lys60 (present in ∼96% of the simulation time with a O−N distance of <3 Å) (Figure 3B). Thus, it appears that Thr11 stabilizes the Cu center in holo-Atox1 by facilitating a network of interactions.

Lys60 in Atox1, located in the α2−β4 loop (Figure 1), is distant in sequence but spatially close in the folded state to the metal binding loop (within 4 Å). This position is always a Lys in eukaryotic Cu chaperones but a Tyr in prokaryotes (*17*). All MBDs except MBD3, which have a Pro, have a Phe at this position (*17*). Because of its positive charge,

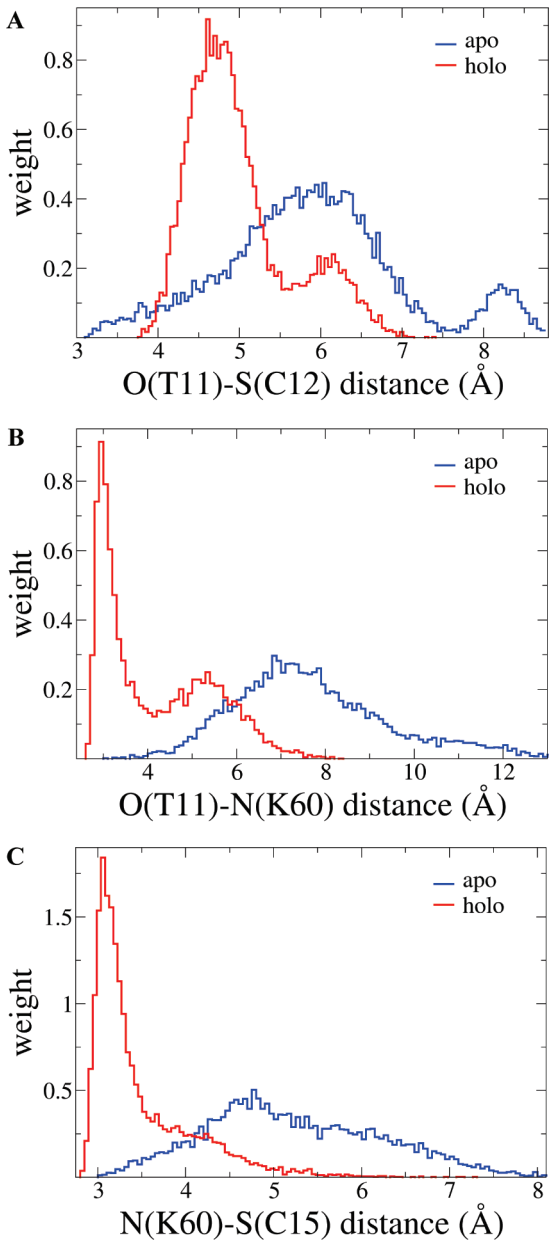

FIGURE 3: Histograms of distance distribution (in angstroms) between heavy atoms of Thr11 (O) and Cys12 (S) (A), Thr11 (O) and Lys60 (N) (B), and Lys60 (N) and Cys15 (S) (C) of WT Atox1 with (red) and without (blue) Cu. Analysis is based on previously published simulation data (*24*).

Lys60 was proposed to contribute to the stabilization of the −1 net charge of the Cu bisthiolate center in the holo form (*17, 26*). In the apo form, Lys60 is flexible and solvent-exposed. Even though its side chain is close to the Cu binding loop, its flexibility impedes stable interactions in the apo form (Figure 3B,C). In holo-Atox1, the flexibility of Lys60 is reduced, and it interacts with the Cu binding loop via strong HBs with Cys15 and Thr11 (Figure 3B,C). This greatly stabilizes the holo form, in particular, the Cu loop and helix α1.

To deduce the individual roles of Met10, Thr11, and Lys60 in Atox1 structural dynamics, we studied the consequences of their replacement with Ala or (for Thr11 and Lys60) with the corresponding prokaryotic residue (described below).

Analysis of Atox1 Variants. (i) Met10Ala. To explore the effect of Met10 removal, we introduced a Met to Ala mutation in silico and subjected the variant to MD simulations in both apo and holo forms. As opposed to WT, Met10Ala Atox1 was simulated for ∼82 and ∼115 ns in the apo and holo forms, respectively (Figure 4A,B). Long times were required for appropriate equilibration of this mutant, as it was found to be more flexible than WT. The backbone rmsd (with respect to the first structure) in the entire simulation was 1.8 ± 0.2 and 1.6 ± 0.3 Å for the apo and holo forms, respectively, suggesting that even though the apo form undergoes more conformational changes, the holo form fluctuates more. To be consistent with the WT data analysis and because the mean backbone rmsd in the last 20 ns was 0.7 ± 0.1 and 0.8 ± 0.2 Å for the apo and holo forms, respectively, the last converged 20 ns of the Met10Ala simulations was used for data analysis.

In general, the backbone is destabilized in the absence of Met10 in both apo and holo forms, especially in the Cu binding loop and helix α1 (Figure 4C,D). This result is consistent with the removed residue being completely buried in the protein core in apo-WT, as opposed to the mutant in which Ala10 does not participate in any important interaction. In terms of structure and backbone dynamics, the largest effect of Met10 removal is found in the apo form. The dynamics of the Cu loop Cys residues in the apo mutant are largely different from those in apo-WT: whereas Cys12 in the loop becomes less floppy, Cys15 in helix α1 becomes more flexible in Met10Ala as compared to WT. Apart from the Cu binding loop and helix α1, the backbone dynamics of apo-Met10Ala is only somewhat increased as compared to that of apo-WT (Figure 4C). Interestingly, residues 40−57, which correspond to strand *β*3, the beginning of helix α2, and their connecting loop, are significantly more rigid in the apo form of Met10Ala as compared to apo-WT. This demonstrates that the effect of the mutation not only is local but also extends through the protein.

Although the differences are subtler in the presence of Cu, holo-Met10Ala also exhibits increased backbone dynamics as compared to holo-WT, and again the greatest change is found in the Cu loop and helix α1 (Figure 4D). The smaller defects observed in this holo mutant as compared to the apo mutant may be explained, in part, by the fact that the Ala10 side chain is buried in holo-Met10Ala. This enables some hydrophobic contacts between Ala10 and the protein core (as opposed to the apo mutant), although not to the same extent as WT (see below). We note that this holo mutant has significant increased flexibility at both ends of the protein, in particular at the C-terminus, which explains its rmsd time evolution (Figure 4B). Also similar to the apo form, residues 43−48, which form the last part of strand *β*3 and the subsequent loop, have their backbone much more restricted in the holo mutant than in holo-WT.

Although the ferredoxin-like fold is intact in apo-Met10Ala, the Cu loop is largely destabilized and changes conformation dramatically, which also extends to the beginning of helix α1 that becomes completely distorted (Figure 5A). These changes involve residues 9−17 and appear to be the result of missing hydrophobic contacts between Met10 and residues in the protein core. In WT Atox1, the Met10 side chain is buried in the core and points toward strands *β*2 and *β*3, where it interacts extensively with residues 33−35 and 38−40. These interactions in WT provide proper packing of the core, which extends to facilitate proper Cu loop

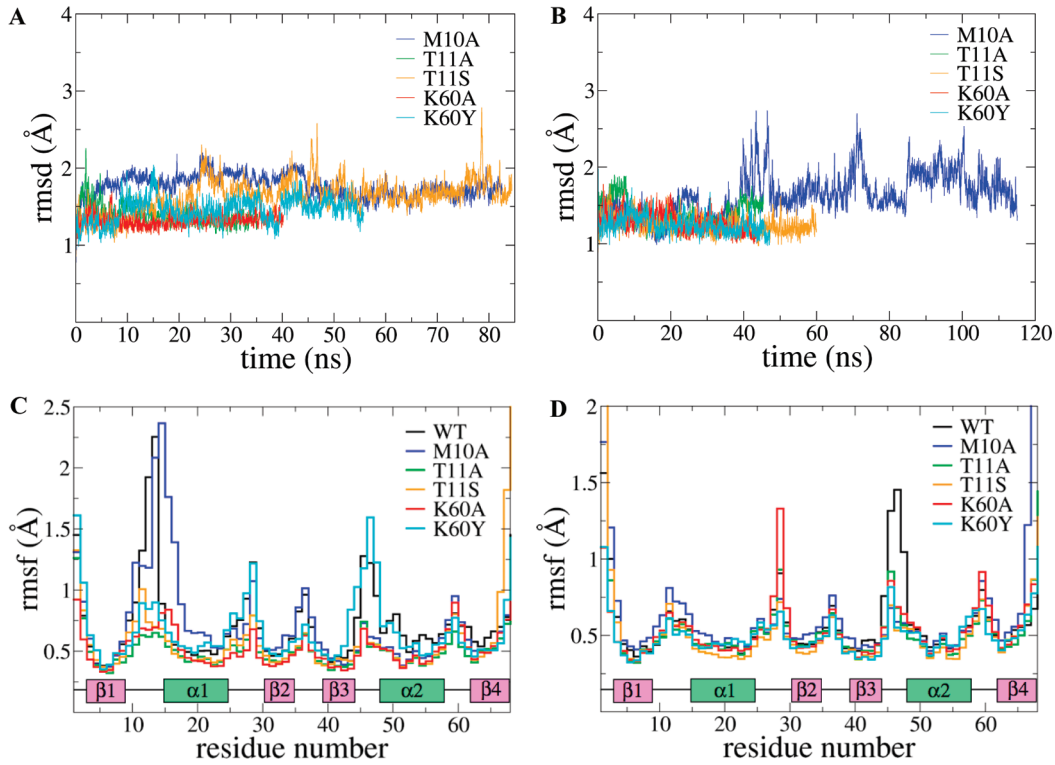

FIGURE 4: (A and B) rmsd (in angstroms, with respect to the first structure) of the backbone heavy atoms (N, Cα, and C) as a function of simulation time for the different variants in apo (A) and holo (B) forms. (C and D) Average fluctuations (rmsf in angstroms) of backbone heavy atoms (N, Cα, and C) per residue (with respect to the first structure of the last 20 ns) for the different variants and WT in apo (C) and holo (D) forms. The secondary structure elements are indicated (α1, α2, and $\beta1-\beta4$): black, WT; blue, Met10Ala; green, Thr11Ala; orange, Thr11Ser; red, Lys60Ala; cyan, Lys60Tyr.

conformation, since Met10 also interacts with Cys15 in helix α1. In apo-Met10Ala, the Ala10 side chain changes orientation, and instead of pointing toward strands $\beta2$ and $\beta3$, it points toward the $\alpha2-\beta4$ loop where it interacts with Thr58 and Lys60. These new interactions contribute to the bending of the Cu loop in this mutant (Figure 5A). Superimposition of the final equilibrated structures of apo-WT and apo-Met10Ala reveals a total rmsd of 1.3 Å, which reduces to 0.6 Å if residues 9−17 are excluded from the calculation. Surprisingly, the lack of key hydrophobic contacts due to the lack of Met10 does not significantly alter the conformation of the Cu loop in the holo form of Met10Ala Atox1. Consequently, the entire structure of holo-Met10Ala is very similar to that of holo-WT, with a total rmsd of only 0.9 Å (Figure 5B). This is probably due to Cu-induced stabilization of the loop, which preserves a correct orientation of Ala10 toward strands $\beta2$ and $\beta3$, as in WT. However, the small Ala10 side chain allows for fewer contacts than WT, extending to only Leu35 and Lys38, explaining the increased backbone dynamics in this region. We note that greater structural changes in apo versus holo forms because of the absence of Met10 was earlier reported for an Atox1 Met10Ser mutant on the basis of 5 ns MD simulations (*25*).

The dynamics and positions of the two Cu binding Cys residues in the apo form of Met10Ala Atox1 differ dramatically from those in apo-WT, as a result of the structural and dynamical alterations observed in this region. Importantly, the S(Cys)−S(Cys) distance distribution changes significantly: whereas WT Atox1 has mainly two populations of distances centered at ∼5.5 and ∼8 Å, the Met10Ala variant has a more diffuse distribution that reaches distances of up to ∼12 Å (Figure 6A). This difference may affect the efficiency of Cu uptake in the mutant, because the Cys will have to rearrange significantly upon Cu binding. Also, apo-Met10Ala gains a HB between Thr11 and Cys12, which is lacking in the apo form of WT (Figure 6B). This interaction may somewhat counteract the overall destabilization of this region in the apo mutant. On the other hand, we find that the Thr11−Cys12 and Lys60−Cys15 interactions found in the WT holo form are not affected by the Met10Ala mutation (Figure 6C,E).

The average proximity to solvent of the Cu loop in Met10Ala Atox1 was analyzed by computing the $g(r)$ between S(Cys12) or S(Cys15), and water (O). Cys12 is solvent-exposed in both apo and holo forms of Met10Ala Atox1, similar to what was found in WT, although Cys12 in apo-Met10Ala Atox1 is slightly more exposed (Figure 7A,B). The Met10Ala mutation does not affect solvent exposure of Cys15 in the holo form, but it results in greater exposure of Cys15 in the apo form (Figure 7C,D). Therefore, in contrast to WT Atox1, the Met10Ala variant buries Cys15 upon Cu binding. An increased level of solvent exposure of Cys15 in apo-Met10Ala may explain the longer S(Cys)−S(Cys) distances observed for this mutant.

(ii) Thr11Ala and Thr11Ser. Thr11 is not a Cu ligand, and although it was proposed to HB with Cys12 of the partner MBDs (*26*), its role in eukaryotic Cu chaperones is not clear. This position is occupied by a Ser in prokaryotic Cu chaperones (*17*), suggesting that a residue capable of forming a HB is necessary. Therefore, we created Thr11Ala and Thr11Ser variants and subjected them to MD simulations in apo and holo forms.

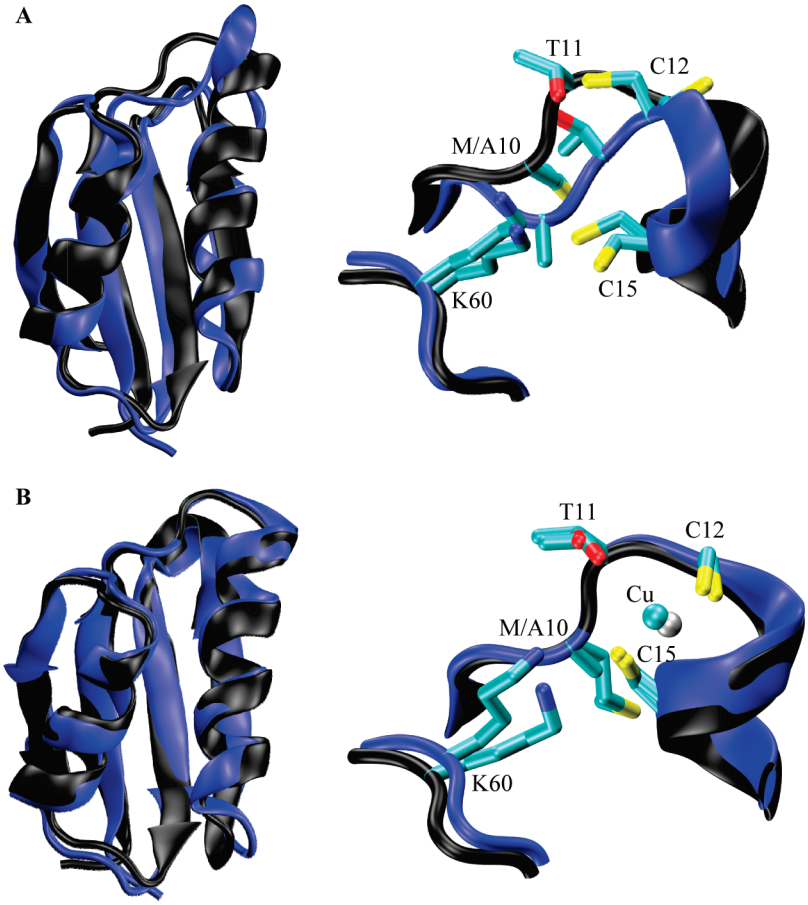

FIGURE 5: Superimposition of the final equilibrated structures of WT (black) and Met10Ala (blue) in the apo (A) and holo (B) forms. A blow-up of the Cu binding loop is shown at the right. Met/Ala10, Thr11, Cys12, Cys15, Lys60, and Cu for each variant are labeled.

Introducing the Thr11Ser mutation was found to have a greater effect than the introduction of Thr11Ala in apo but not in holo forms. Thr11Ala Atox1 apo and holo forms were simulated for ~35 and ~45 ns, respectively, with a total rmsd of 1.4 ± 0.1 Å (Figure 4A,B). In the last 20 ns, both forms are stable with mean rmsds of 0.54 ± 0.08 and 0.7 ± 0.1 Å, respectively. Because of its increased flexibility, apo-Thr11Ser required longer simulation times, ~84 ns, with a total rmsd of 1.6 ± 0.2 Å (Figure 4A). However, it was stable in the last 20 ns, with a mean rmsd of 0.7 ± 0.1 Å. On the other hand, holo-Thr11Ser exhibited smaller conformational changes (total rmsd of 1.2 ± 0.1 Å) and reached equilibrium faster than the apo form; it was simulated for ~60 ns with a mean rmsd of 0.6 ± 0.1 Å in the last 20 ns.

Like what we observed for Met10Ala, the Thr11 mutations have greater effects on Atox1 backbone flexibility in the absence of Cu (Figure 4C,D). The backbone motion of the entire protein, also in regions far from the mutation, is greatly reduced by both substitutions in the apo form as compared to apo-WT. The greatest changes are found in the Cu loop and in helix α1, which results in less mobility of the two Cu-coordinating Cys residues. In this region, the stiffening effect is largest for the Thr11Ala mutant; however, in the rest of the protein, both mutants have similar backbone dynamics. Similar to what we observed for Met10Ala, residues 44−57 are significantly less flexible in the Thr11 mutants than in apo-WT. In WT apo-Atox1, the methyl group (CG) of Thr11 is solvent-exposed and close to the N atom of Lys38. This proximity of a hydrophobic and a polar group may significantly increase the entropy of the loop. In the Thr mutants, the loop becomes "frozen" due to the absence of this entropic effect. Despite the changes in backbone flexibility, the overall fold is essentially unaltered in the apo forms of the two Thr mutants (Figure 8A), with a total rmsd with respect to apo-WT of 0.8 and 1.2 Å for Thr11Ala and Thr11Ser, respectively.

The effect of the mutations in terms of protein and loop dynamics is smaller in the holo form (Figure 4D) because Cu binding stabilizes the Cu loop in WT Atox1. However, the backbones of both holo mutants are more rigid that in holo-WT; the effect is largest for residues 40−55. Because of the dramatic reduction in the flexibility of apo-Thr11Ala, this mutant undergoes only a slight stabilization of the Cu loop upon Cu binding, whereas Thr11Ser is more markedly stabilized. The folds of the holo variants are similar to those of holo-WT, with rmsds with respect to WT of 0.9 and 0.8 Å for Thr11Ala and Thr11Ser, respectively (Figure 8B).

The S(Cys)−S(Cys) distance distribution is not greatly altered in the Thr11Ala apo mutant: during most of the simulation time (~70%) it is ~5.5 Å, which is similar to the distance in WT (Figure 6A). On the other hand, the Thr11Ser apo mutant exhibits most of the time (~60%) a shorter S−S distance of ~3.5 Å. We previously proposed that a "stretched" Cys conformation, in which the S(Cys)−S(Cys) distance is ~8 Å, may be important for initial Cu uptake. Shorter S(Cys)−S(Cys) distances, like the ones found here for the Thr11Ser variant, may increase the probability of formation of a disulfide bond (which would block Cu uptake).

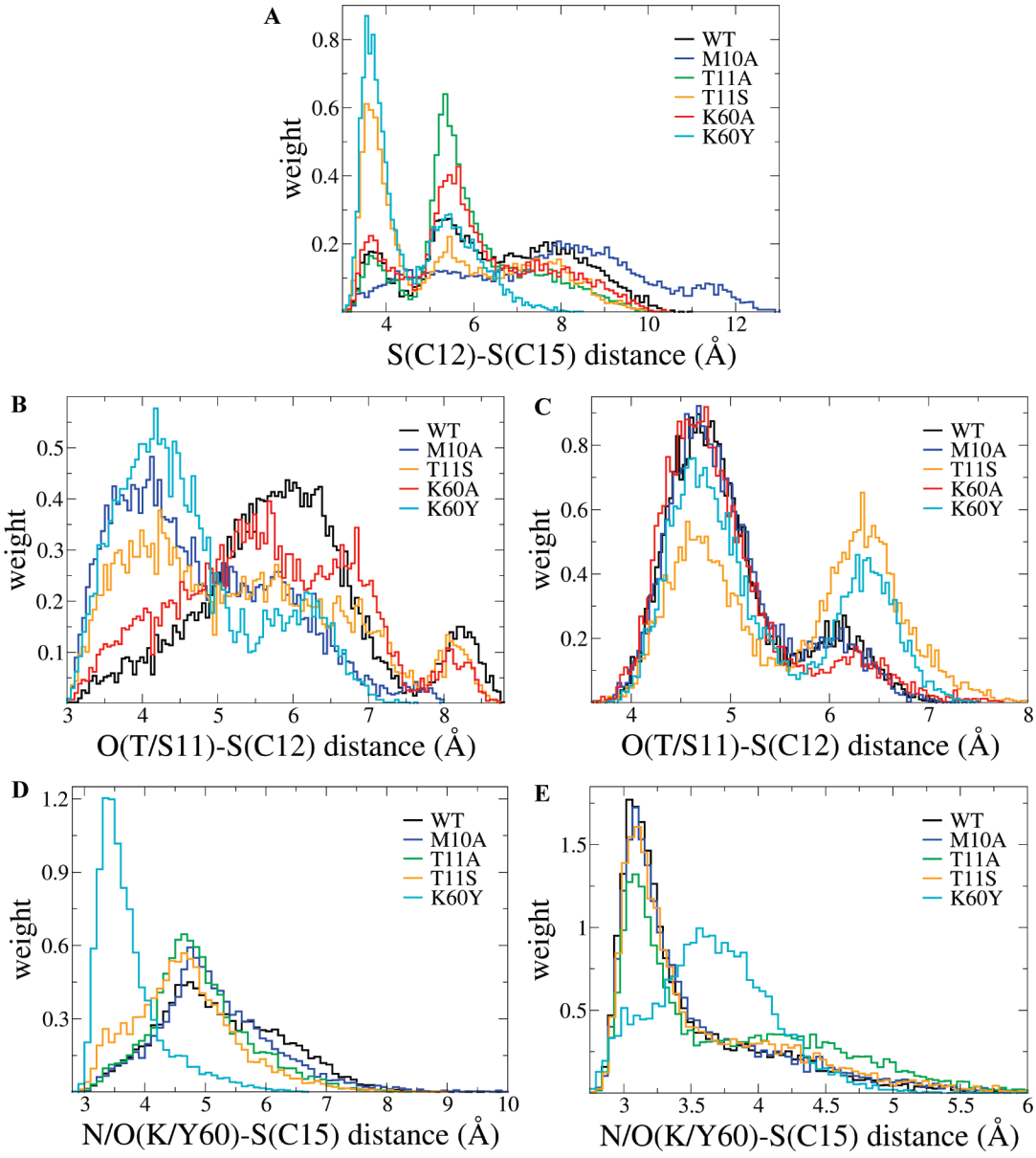

FIGURE 6: Histograms of distance distribution (in angstroms) between heavy atoms of Cys12 (S) and Cys15 (S) in the apo form (A), Thr/Ser11 (O) and Cys12 (S) in apo (B) and holo (C) forms, and Lys/Tyr60 (N/O) and Cys15 (S) in apo (D) and holo (E) forms, for the different variants and WT: black, WT; blue, Met10Ala; green, Thr11Ala; orange, Thr11Ser; red, Lys60Ala; cyan, Lys60Tyr.

Thr11Ala Atox1 lacks the ability of residue 11 to HB with Cys12 or Lys60, whereas the Thr11Ser variant retains this ability. As in Met10Ala but different from WT Atox1, in Thr11Ser, Ser11 forms a HB with Cys12 in the apo form (Figure 6B). Formation of this HB in apo-Thr11Ser results in a different orientation of Cys12: this can explain the reduced S(Cys)−S(Cys) distance observed in this mutant. The Ser11−Cys12 interaction appears to be the principal cause of all alterations found for apo-Thr11Ser but not for apo-Thr11Ala (see also Cys exposure below). In apo-WT, an interaction between Thr11 and Cys12 does not occur (Figure 3A) because of the high flexibility in this region. In holo-WT, Thr11 HBs to Lys60 ~96% of the simulation time; this facilitates an interaction between Thr11 and Cys12 (Figure 3A,B). Although Thr11Ser is still capable of forming HBs, in this case the HB between Ser11 and Lys60 is only present ~55% of the time. This in turn weakens the electrostatic interaction between Ser11 and Cys12 in holo-Thr11Ser, where they interact only ~50% versus ~90% of the time in WT (Figure 6C). The interaction between Lys60 and Cys15 found in the WT holo form is not affected in Thr11Ser. However, in Thr11Ala, the Lys60 side chain fluctuates farther from the Cu site, which weakens the HB between this residue and Cys15 (Figure 6E). Thus, it appears that both Thr11 mutants result in weakening of the electrostatic network surrounding the Cu center, which may destabilize the Cu-bound state.

In the apo form, Cys solvent exposure changes only in the Thr11Ser mutant: whereas Cys12 is more buried, Cys15 is significantly more exposed in Thr11Ser than in apo-WT (Figure 7A,C). This correlates well with the alteration in S(Cys)−S(Cys) distance distribution observed only for the Thr11Ser variant. In the holo forms, solvation of the Cu-coordinating Cys residues is not altered by any mutation of Thr11 (Figure 7B,D). Because of this difference between

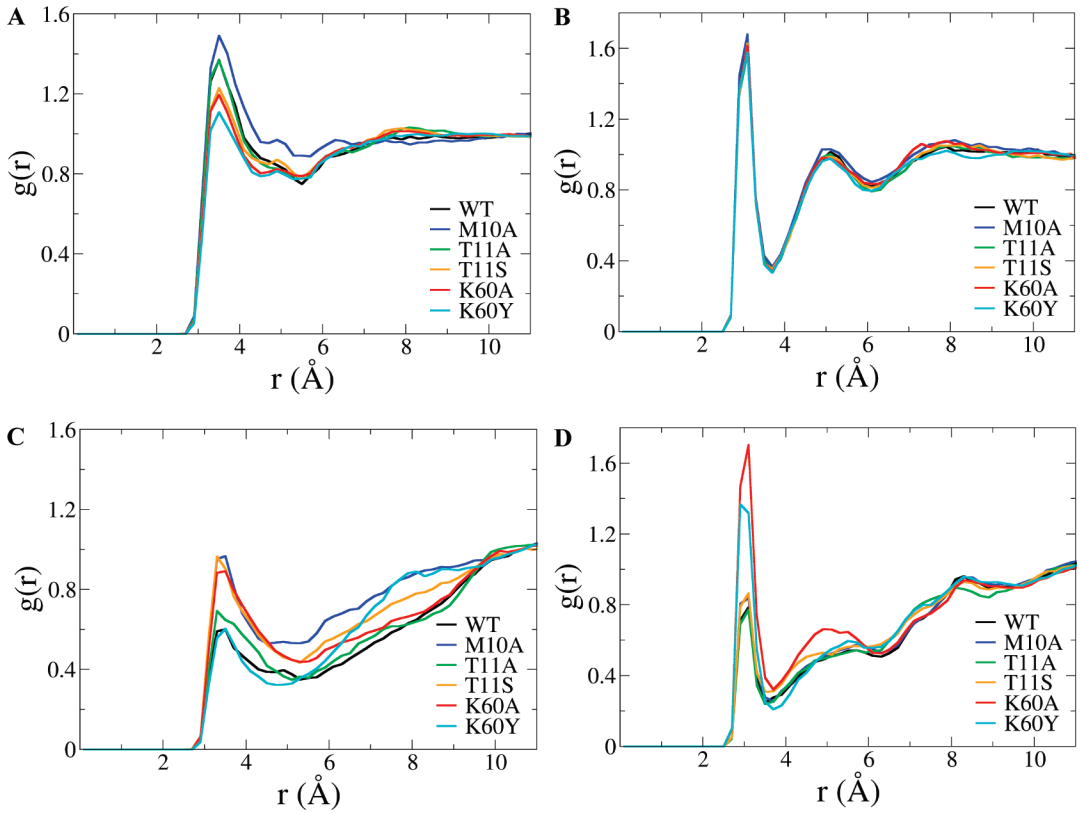

FIGURE 7: Protein−solvent radial distribution functions $g(r)$ of Cys12 in apo (A) and holo (B) forms and Cys15 in apo (C) and holo (D) forms, for the different Atox1 variants and WT: black, WT; blue, Met10Ala; green, Thr11Ala; orange, Thr11Ser; red, Lys60Ala; cyan, Lys60Tyr.

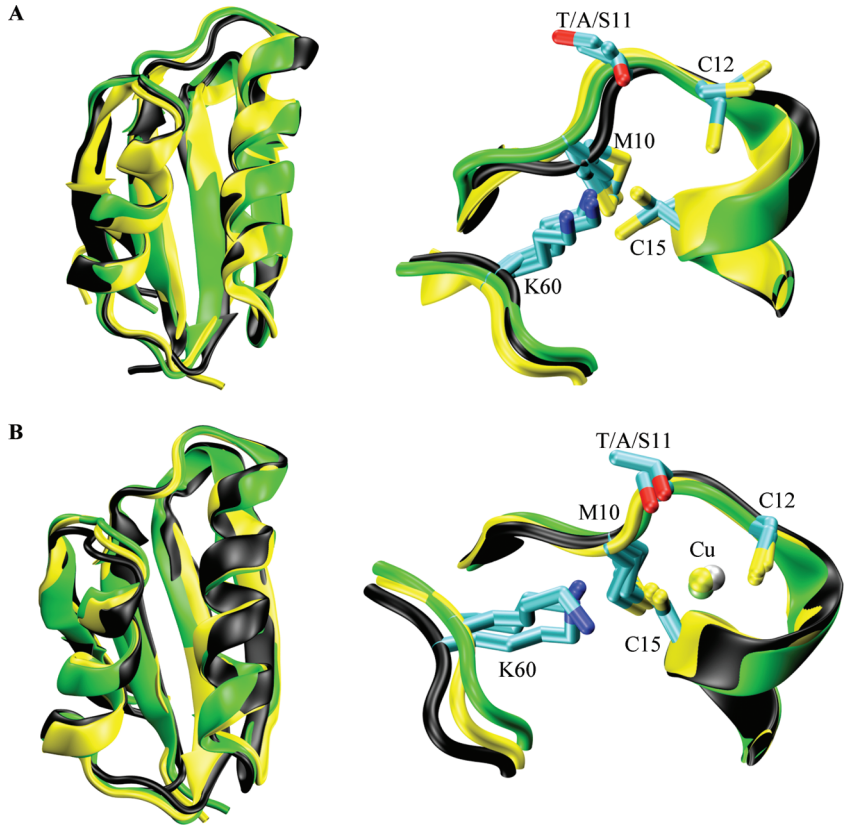

FIGURE 8: Superimposition of the final equilibrated structures of WT (black), Thr11Ala (green), and Thr11Ser (yellow) in the apo (A) and holo (B) forms. A blow-up of the Cu binding loop is shown at the right. Met10, Thr/Ala/Ser11, Cys12, Cys15, Lys60, and Cu for each variant are labeled.

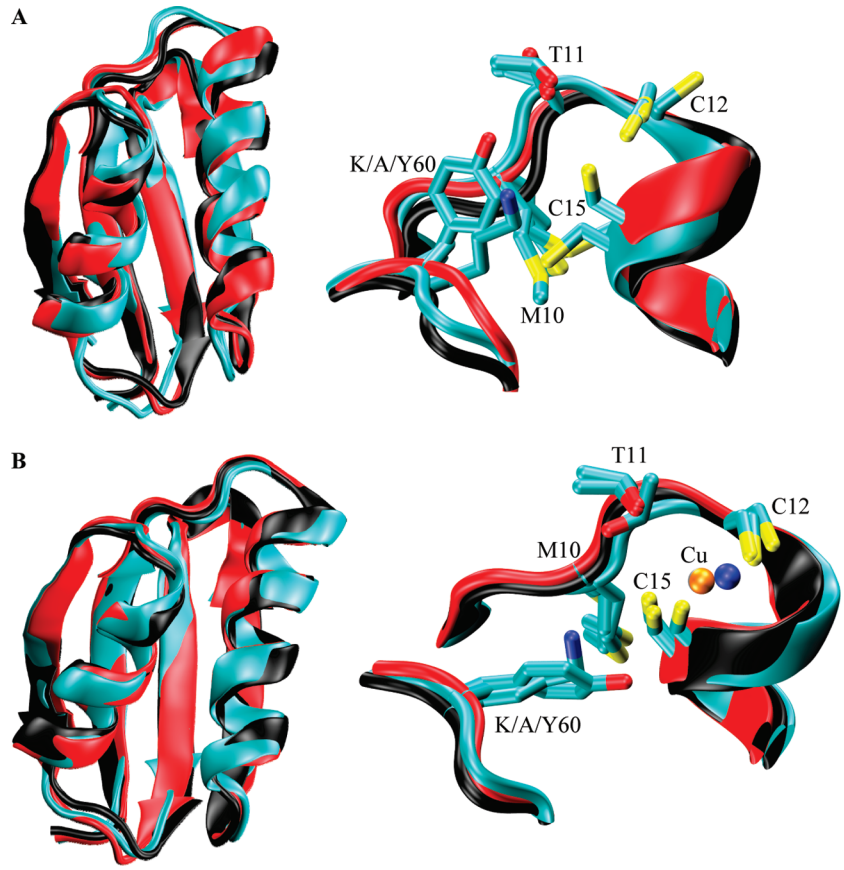

FIGURE 9: Superimposition of the final equilibrated structures of WT (black), Lys60Ala (red), and Lys60Tyr (cyan) in the apo (A) and holo (B) forms. A blow-up of the Cu binding loop is shown at the right. Met10, Thr11, Cys12, Cys15, Lys/Ala/Tyr60, and Cu for each variant are labeled.

apo and holo forms, in Thr11Ser Atox1 Cys15 becomes more buried, instead of more exposed, upon Cu binding.

(iii) Lys60Ala and Lys60Tyr. To analyze the role of Lys60 in Atox1, we created Lys60Ala and Lys60Tyr variants and subjected them to MD simulations with and without Cu. The Lys60Tyr mutant was created to mimic the bacterial homologues.

The Lys60 mutants are stabilized quite fast, except for apo-Lys60Tyr that required a longer time (Figure 4A,B). Lys60Ala was simulated for ~40 and ~44 ns and Lys60Tyr for ~55 and ~47 ns in the absence and presence of Cu, respectively. These proteins exhibited the smallest conformational changes of all Atox1 variants, with a total rmsd of 1.3 ± 0.1 Å for apo- and holo-Lys60Ala and rmsds of 1.5 ± 0.2 and 1.2 ± 0.1 Å for the corresponding forms of Lys60Tyr, respectively. All proteins were very stable in the last 20 ns of production simulations, with mean rmsds of 0.5 ± 0.1, 0.56 ± 0.09, 0.7 ± 0.1, and 0.5 ± 0.1 Å for apo-Lys60Ala, holo-Lys60Ala, apo-Lys60Tyr, and holo-Lys60Tyr, respectively.

As for the other Atox1 mutants, the greatest effect of the Lys substitutions is observed in the absence of Cu. For both apo forms, the proteins become less flexible, especially in the Cu loop and helix α1 (Figure 4C). Lys60Ala flexibility is similar to that of the Thr11 mutants and is dramatically lower than that in WT, the effect extending throughout the entire protein. On the other hand, Lys60Tyr flexibility is closer to WT behavior, as this mutant is mostly rigidified in the Cu loop. Nonetheless, the folds of the apo mutants are the same as that of WT, with rmsds of only 0.9 and 1.3 Å for Lys60Ala and Lys60Tyr, respectively (Figure 9A). In WT Atox1, even though Lys60 does not HB to Cys15 and has increased conformational flexibility in the apo form, the side chain of Lys60 fluctuates near the Cu loop. The presence of this bulky, charged, and flexible residue toward the Cu loop seems to increase the entropy of this loop in apo-WT. On the other hand, in apo-Lys60Ala, the side chain of Ala60 points toward the protein core. The extra hydrophobic contacts made in Lys60Ala stabilize not only the Cu loop but also the entire backbone. In apo-Lys60Tyr, Tyr60 is also close to the Cu loop, like Lys60 in WT, but has reduced flexibility and interacts extensively with Ala18 and Cys15 in helix α1 (Figure 6D). This stable and strong HB between Tyr60 and Cys15 in apo-Lys60Tyr greatly stabilizes the Cu loop and the beginning of helix α1 but does not affect the core. Thus, addition of Ala at position 60 affects the whole protein, whereas addition of Tyr has mainly a local effect in the loop.

In the presence of Cu, both Lys60 mutants appear rather similar to WT in terms of backbone fluctuations except for some regions (Figure 4D). Both holo mutants have restricted motion of residues 40−50, which was also observed for the other Atox1 mutants. Also, the holo form of Lys60Ala exhibits increased flexibility in the α1−β2 loop, resulting in a greater mobility of this region upon Cu binding, as opposed to WT and Lys60Tyr. On the other hand, the Cu loop is stabilized in Lys60Ala upon Cu binding but not as much as in Lys60Tyr, which is more WT-like. Thus, it appears that whereas an Ala at position 60 is not tolerated, the prokaryotic residue, Tyr, can maintain part of the WT

Table 1: Summary of the Most Significant Changes in the Different Mutants with Respect to WT Atox1[a]

		backbone flexibility	Cys−Cys distance	interactions	Cys exposure
apo	M10A	+	+	HB T11−C12/loss of core interactions	C12+, C15+
	T11A	−	WT	WT	C15+
	T11S	−	−	HB S11−C12	C12−, C15+
	K60A	−	WT	WT	C12−, C15+
	K60Y	−	−	HB T11−C12 and Y60−C15	C12−
holo	M10A	+	NA	loss of core interactions	WT
	T11A	−	NA	loss of HB T11−K60 and T11−C12/weak HB K60−C15	WT
	T11S	−	NA	weak HB S11−K60 and S11−C12	WT
	K60A	−	NA	loss of HB K60−C15	C15+
	K60Y	−	NA	weak HB T11−Y60, T11−C12, and Y60−C15	C15+

[a] Legend: +, increase; −, decrease with respect to WT of backbone flexibility, length of Cys−Cys distance, and Cys solvent exposure. WT means wild-type-like behavior of that property. In apo-WT, there is no HB between T11 and C12 and no HB between K60 and C15. In holo-WT, there is a HB between T11 and K60, electrostatic interaction between T11 and C12, and a HB between K60 and C15. In both WT forms, Met10 interacts with the hydrophobic core.

Atox1 behavior. Structurally, both holo mutants are identical to the WT holo form, with rmsd values of 0.7 and 0.6 Å for Lys60Ala and Lys60Tyr Atox1, respectively (Figure 9B).

In apo-Lys60Ala, the S(Cys)−S(Cys) distance is not much perturbed as compared to that in WT (Figure 6A). On the other hand, in apo-Lys60Tyr, most of the simulation time (∼85%), the S−S distance is shorter, ∼3.5 Å. In Lys60Tyr, but not in Lys60Ala Atox1, a HB is formed between Thr11 and Cys12 in the apo form (Figure 6B). As in the Thr11Ser mutant, formation of this unique HB in apo-Lys60Tyr results in a different conformation of Cys12, which may explain the altered Cys−Cys distance distribution in this mutant (but not in the apo form of Lys60Ala Atox1). On the other hand, there is a weakening of such electrostatic interaction around the Cu center in holo-Lys60Tyr as compared to holo form of WT Atox1 (Figure 6C). Lys60Ala is unable to provide a HB to Cys15, and thus, this holo variant lacks an important electrostatic component that stabilizes the Cu center. Whereas Tyr60 in holo-Lys60Tyr is capable of providing such a bond, it does not occur as frequently as in the holo form of WT Atox1 (Figure 6E). However, this interaction is present in the apo form of Lys60Tyr Atox1 but not in apo-WT Atox1 (Figure 6D), which contributes to stabilization of the Cu loop in the mutant as mentioned above. Altogether, these findings point to a role of Lys60 in preserving an electrostatic network around the Cu site of Atox1.

Solvation of the Cu-coordinating Cys residues markedly changes in the two Tyr60 mutants. In the apo forms, Cys12 is less solvent exposed in both mutants as compared to the apo form of WT Atox1 (Figure 7A). Because Cys12 is proposed to be the first sulfur ligand to bind Cu (*39*), shielding of this residue may affect Cu binding parameters. Whereas Cys15 exposure appears not to be affected in apo-Lys60Tyr, it becomes more exposed in the apo form of Lys60Ala Atox1 (Figure 7C). In the presence of Cu, Cys15 is much more exposed to solvent in both mutants, accompanied by the gain of a HB with water (Figure 7D). As a consequence, Cu is less shielded in these mutants; this makes the Cu−Cys15 bond more susceptible for attack by water or another protein.

(iv) Cross Correlation Analysis of Atox1 Variants. The cross correlation matrices of apo and holo forms of each Atox1 variant were also calculated (data not shown). The data indicate that all positive cross correlations that maintain the ferredoxin-like fold in WT Atox1 are conserved in the variants, consistent with the small effects of all mutations seen in the rmsd time evolution data. Interestingly, in all the apo mutants, the out-of-phase coupling between structural elements within the blue (involving residues in the Cu loop side of the protein) and green (involving residues in the opposite side of the Cu loop) regions (Figure 2A) is completely (in Thr11Ala, Thr11Ser, and Lys60Ala) or nearly (in Met10Ala and Lys60Tyr) lost. Also, in contrast to that in WT holo-Atox1, none of the holo mutants exhibit any significant negative cross correlations. These results demonstrate that the specific pattern of anticorrelation between residues in the Cu loop and nearby residues in WT apo-Atox1 is disrupted by the mutations. Because all mutations alter the Cu loop flexibility to some extent, we can conclude that the intrinsic flexibility of this loop in apo-Atox1 is necessary to induce specific concerted motions, which may be necessary for Cu binding. Because of the absence of concerted motions in the holo mutants, the mutations may also cause alterations in protein−protein interactions and/or in efficiency of Cu release.

CONCLUSIONS AND SIGNIFICANCE

We have assessed the consequences of removing, one by one, three residues in Atox1. None of the residues are interacting with the Cu; nonetheless, they are all conserved. Met10 is conserved in all kingdoms of life, including Cu chaperones and MBDs, whereas Thr11 and Lys60 are only conserved as such in eukaryotic Cu chaperones (*17*). In prokaryotic Cu chaperones, Thr11 is a Ser and Lys60 is a Tyr. We have simulated Met10Ala, Thr11Ala, Thr11Ser, Lys60Ala, and Lys60Tyr variants of Atox1 in apo and holo forms, resulting in a total simulation time of ∼600 ns, to obtain a detailed description of the effects of Met10, Thr11, and Lys60 on Cu loop properties, overall protein flexibility, S(Cys)−S(Cys) distance, solvent exposure of the functional Cys, and correlated protein fluctuations. The most important differences found in the variants with respect to WT Atox1 are summarized in Table 1.

Interestingly, all substitutions in Atox1 resulted in subtle effects, affecting mainly the Cu loop structure and dynamics, but the overall fold is conserved. This points to the robustness of the ferredoxin-like fold and is consistent with purified Met10Ala, Lys60Ala (*41*), Lys60Tyr, and Thr11Ala (F. Hussain and P. Wittung-Stafshede, unpublished data) Atox1 variants having far-UV CD and fluorescence emission signals similar to those of WT Atox1 (*41*). We find here that, in terms of backbone flexibility, all substitutions have the largest

effects in the apo form. It appears thus that the binding of Cu to the proteins overrules structural or dynamic "defects" in the apo variants. Despite individual differences, all apo forms are more floppy than the corresponding holo forms, as also found for WT Atox1 (*24*). This correlates with in vitro thermal unfolding experiments on purified proteins, which indicate that Met10Ala, Thr11Ala, Lys60Ala, and Lys60Tyr Atox1 variants are more stable in the presence of Cu (F. Hussain and P. Wittung-Stafshede, unpublished data), which was found previously for WT Atox1 (*27*).

Each Atox1 variant studied here has a unique in silico behavior, which allows dissection of the role of each residue in Atox1 structure and dynamics. Nonetheless, general trends among the variants also emerge from our simulation data. Deletion of Met10 in Atox1 disrupts the core of Atox1, and the Met10Ala variant is more floppy than WT. We find that Met10 participates in several hydrophobic interactions in the core, which stabilizes the overall fold. Proper packing of the fold in turn contributes to an optimal Cu binding loop conformation. In accord with our MD data, in vitro studies on purified Met10Ala Atox1 in apo and holo forms demonstrate that both forms have lower thermal stability than WT Atox1 (F. Hussain and P. Wittung-Stafshede, unpublished data). Moreover, the increase in backbone and Cu loop flexibility of Met10Ala explains the reported rapid release of Cu from holo-Met10Ala Atox1 to BCA (*41*). Interestingly, Met10 appears to keep Cys15 relatively buried in the apo form, which results in an intermediate Cys−Cys distance in WT Atox1. The Met10Ala Atox1 mutant has its Cys residues much farther from each other, which predicts that the Cys will have to rearrange significantly to be able to coordinate Cu. This finding is consistent with the reported slower rate of binding of the Cu−BCA complex to apo-Met10Ala Atox1 (*41*).

To our surprise, the Thr- and Lys-deleted variants are more rigid than WT Atox1. The effect is most dramatic in the apo forms; in presence of Cu, all holo forms have restricted motion. This finding implies that the presence of these two residues increases the entropy of WT Atox1; in particular, they significantly increase the backbone fluctuations of the Cu loop. Thr11 has its hydrophobic methyl group (CG) exposed to solvent, and the Lys60 side chain fluctuates close to the Cu loop; both these features seem to contribute to increasing Cu loop flexibility in apo-WT. Proper plasticity of the Cu loop and thereby an appropriate distance between and solvent exposure of the two Cys residues may be necessary for efficient Cu uptake in vivo. Our in silico finding of increased stiffness in the Thr and Lys variants is consistent with in vitro studies of purified Thr11Ala and Lys60Ala Atox1 variants. In both apo and holo forms, these mutants have higher thermal midpoints than WT Atox1 (F. Hussain and P. Wittung-Stafshede, unpublished data). Also, in our simulations, most Thr and Lys apo mutants have Cys12 more buried than in WT. Because Cys12 is the first Cys proposed to interact with Cu (*39*), burial of Cys12 in the mutants may affect Cu uptake speed and/or efficiency, as the Cys may need to rearrange to accommodate the metal. This is consistent with the reported lower rate of binding of the Cu−BCA complex to apo-Lys60Ala Atox1, as also observed for Met10Ala (*41*).

Furthermore, from the simulation data on the holo forms of the Thr and Lys mutants, it is clear that these residues are important in forming an electrostatic network around the Cu site. Both Thr11 and Lys60 stabilize the Cu-bound state by hydrogen bonding with key residues in the metal binding loop. Interestingly, Lys60 also protects Cys15 from solvent in the holo form, shielding the Cu site. We recently reported experimental kinetic work that demonstrated that Cu is more easily displaced from Lys60Ala Atox1 by BCA, than from WT, due to the higher affinity of the first BCA and more rapid dissociation of Atox1 from the transient Atox1−Cu−BCA complex (*41*). The greater rigidity of the Cu loop and exposure of Cys15 in holo-Lys60Ala found here may explain why the first BCA binds more efficiently and the mutant dissociates faster than WT, respectively. It appears that proper solvation of the Cys residues that coordinate Cu is important for facilitating Cu uptake and release. The Cys should be sufficiently solvent exposed in the apo form to ensure timely uptake of Cu but buried enough in the holo form to avoid premature loss of Cu.

Although the prokaryotic residues, Ser and Tyr, at first sight appear to be good replacements for the corresponding eukaryotic residues, Thr11Ser and Lys60Tyr variants of Atox1 did not behave like WT. In the case of residue 60, Tyr is tolerated better than Ala in both apo and holo forms. In the apo form, this is because the small side chain of Ala becomes buried in the hydrophobic core, which greatly stabilizes the entire backbone, whereas Tyr60 stabilizes only the Cu binding loop. In the holo form, Tyr can form a HB to Cys15 whereas Ala60 cannot. On the other hand, whereas Ser11 was tolerated better than Ala11 in holo-Atox1, Ala was a better replacement in the apo form. In the apo forms, although both mutations rigidified the protein to similar extents, Thr11Ser is involved in a HB that is absent in WT and Thr11Ala forms of Atox1, which alters the dynamics and solvent exposure of the Cys residues. In holo-Atox1, however, Ser11, but not Ala11, can substitute for Thr11 by forming a HB with Lys60. This interaction may explain the presence of His in position X_1 in MBD3 of ATP7A and ATP7B (*17*). Importantly, in both Thr11Ser and Lys60Tyr, but not in any other variant, the Cys−Cys distance became shorter in the apo form. We previously speculated about a stretched Cys conformation that would allow for easy "pull-in" of Cu (*24*). It is possible that Thr11 and Lys60 play roles in optimizing the Cys−Cys distance distribution in Atox1 by their interactions with the Cys residues. Differences in Cu transfer mechanisms, protein partners, and protein−metal affinities may explain the presence of Ser and Tyr in bacterial Cu chaperones.

Finally, we previously showed that in WT forms of Atox1 and CopZ the $\beta3-\alpha2$ loop, which is located at the opposite side of the Cu loop, was the only region that becomes more floppy upon Cu binding, and we proposed that conformational changes in this loop may mediate protein−protein interactions (*24*). In all Atox1 mutants tested here, in contrast to WT Atox1, this region either did not change at all or became more structured upon Cu binding. In addition, all apo mutants exhibited significantly less negative cross correlation in this region as compared to the WT apo form. This may imply that the studied residues, in addition to facilitating Cu uptake and release, are important for providing appropriate chaperone−partner interactions in the cell.

To understand biological transfer of Cu from Atox1 to target domains, one must first understand the biophysics of

the individual proteins. This study provides a comprehensive in silico analysis of the roles of three conserved residues in the structure and dynamics of the human Cu chaperone Atox1. Our findings emphasize the importance of Cu binding loop flexibility for Atox1 biological activity. Thus, during evolution of functional Cu chaperones, residues lowering protein stability and increasing backbone flexibility appear to have been added onto the rigid ferredoxin-like scaffold. This property may be required to form Cu-bridged hetero-protein complexes with target domains in vivo. Future NMR spin relaxation experiments on the Atox1 mutants characterized here could be used to validate our in silico findings experimentally, as by this approach protein residue dynamics can be detected on similar time scales as reported here (i.e., picoseconds to nanoseconds).

ACKNOWLEDGMENT

We thank Dr. Alejandro Crespo for useful discussions and Faiza Hussain for sharing thermal unfolding data on Atox1 mutants.

REFERENCES

1. O'Halloran, T. V., and Culotta, V. C. (2000) Metallochaperones, an intracellular shuttle service for metal ions. *J. Biol. Chem. 275*, 25057–25060.
2. Huffman, D. L., and O'Halloran, T. V. (2001) Function, structure, and mechanism of intracellular copper trafficking proteins. *Annu. Rev. Biochem. 70*, 677–701.
3. Puig, S., Rees, E. M., and Thiele, D. J. (2002) The ABCDs of periplasmic copper trafficking. *Structure 10*, 1292–1295.
4. Puig, S., and Thiele, D. J. (2002) Molecular mechanisms of copper uptake and distribution. *Curr. Opin. Chem. Biol. 6*, 171–180.
5. Harris, E. D. (2003) Basic and clinical aspects of copper. *Crit. Rev. Clin. Lab. Sci. 40*, 547–586.
6. Rosenzweig, A. C., and O'Halloran, T. V. (2000) Structure and chemistry of the copper chaperone proteins. *Curr. Opin. Chem. Biol. 4*, 140–147.
7. Harrison, M. D., Jones, C. E., Solioz, M., and Dameron, C. T. (2000) Intracellular copper routing: The role of copper chaperones. *Trends Biochem. Sci. 25*, 29–32.
8. Hamza, I., Schaefer, M., Klomp, L. W., and Gitlin, J. D. (1999) Interaction of the copper chaperone HAH1 with the Wilson disease protein is essential for copper homeostasis. *Proc. Natl. Acad. Sci. U.S.A. 96*, 13363–13368.
9. Hung, I. H., Casareno, R. L., Labesse, G., Mathews, F. S., and Gitlin, J. D. (1998) HAH1 is a copper-binding protein with distinct amino acid residues mediating copper homeostasis and antioxidant defense. *J. Biol. Chem. 273*, 1749–1754.
10. Klomp, L. W., Lin, S. J., Yuan, D. S., Klausner, R. D., Culotta, V. C., and Gitlin, J. D. (1997) Identification and functional expression of HAH1, a novel human gene involved in copper homeostasis. *J. Biol. Chem. 272*, 9221–9226.
11. Hung, I. H., Suzuki, M., Yamaguchi, Y., Yuan, D. S., Klausner, R. D., and Gitlin, J. D. (1997) Biochemical characterization of the Wilson disease protein and functional expression in the yeast *Saccharomyces cerevisiae*. *J. Biol. Chem. 272*, 21461–21466.
12. Hellman, N. E., Kono, S., Mancini, G. M., Hoogeboom, A. J., De Jong, G. J., and Gitlin, J. D. (2002) Mechanisms of copper incorporation into human ceruloplasmin. *J. Biol. Chem. 277*, 46632–46638.
13. Gitlin, J. D. (2003) Wilson disease. *Gastroenterology 125*, 1868–1877.
14. Tao, T. Y., and Gitlin, J. D. (2003) Hepatic copper metabolism: Insights from genetic disease. *Hepatology 37*, 1241–1247.
15. Kulkarni, P. P., She, Y. M., Smith, S. D., Roberts, E. A., and Sarkar, B. (2006) Proteomics of metal transport and metal-associated diseases. *Chemistry 12*, 2410–2422.
16. Miyajima, H., Takahashi, Y., Kamata, T., Shimizu, H., Sakai, N., and Gitlin, J. D. (1997) Use of desferrioxamine in the treatment of aceruloplasminemia. *Ann. Neurol. 41*, 404–407.
17. Arnesano, F., Banci, L., Bertini, I., Ciofi-Baffoni, S., Molteni, E., Huffman, D. L., and O'Halloran, T. V. (2002) Metallochaperones and metal-transporting ATPases: A comparative analysis of sequences and structures. *Genome Res. 12*, 255–271.
18. DeSilva, T. M., Veglia, G., and Opella, S. J. (2005) Solution structures of the reduced and Cu(I) bound forms of the first metal binding sequence of ATP7A associated with Menkes disease. *Proteins 61*, 1038–1049.
19. Banci, L., Bertini, I., Ciofi-Baffoni, S., Huffman, D. L., and O'Halloran, T. V. (2001) Solution structure of the yeast copper transporter domain Ccc2a in the apo and Cu(I)-loaded states. *J. Biol. Chem. 276*, 8415–8426.
20. Banci, L., Bertini, I., Del Conte, R., Markey, J., and Ruiz-Duenas, F. J. (2001) Copper trafficking: The solution structure of *Bacillus subtilis* CopZ. *Biochemistry 40*, 15660–15668.
21. Pufahl, R. A., Singer, C. P., Peariso, K. L., Lin, S. J., Schmidt, P. J., Fahrni, C. J., Culotta, V. C., Penner-Hahn, J. E., and O'Halloran, T. V. (1997) Metal ion chaperone function of the soluble Cu(I) receptor Atx1. *Science 278*, 853–856.
22. Rosenzweig, A. C., Huffman, D. L., Hou, M. Y., Wernimont, A. K., Pufahl, R. A., and O'Halloran, T. V. (1999) Crystal structure of the Atx1 metallochaperone protein at 1.02 Å resolution. *Structure 7*, 605–617.
23. Arnesano, F., Banci, L., Bertini, I., Huffman, D. L., and O'Halloran, T. V. (2001) Solution structure of the Cu(I) and apo forms of the yeast metallochaperone, Atx1. *Biochemistry 40*, 1528–1539.
24. Rodriguez-Granillo, A., and Wittung-Stafshede, P. (2008) Structure and Dynamics of Cu(I) Binding in Copper Chaperones Atox1 and CopZ: A Computer Simulation Study. *J. Phys. Chem. B 112*, 4583–4593.
25. Poger, D., Fuchs, J. F., Nedev, H., Ferrand, M., and Crouzy, S. (2005) Molecular dynamics study of the metallochaperone Hah1 in its apo and Cu(I)-loaded states: Role of the conserved residue M10. *FEBS Lett. 579*, 5287–5292.
26. Wernimont, A. K., Huffman, D. L., Lamb, A. L., O'Halloran, T. V., and Rosenzweig, A. C. (2000) Structural basis for copper transfer by the metallochaperone for the Menkes/Wilson disease proteins. *Nat. Struct. Biol. 7*, 766–771.
27. Hussain, F., and Wittung-Stafshede, P. (2007) Impact of cofactor on stability of bacterial (CopZ) and human (Atox1) copper chaperones. *Biochim. Biophys. Acta 1774*, 1316–1322.
28. Anastassopoulou, I., Banci, L., Bertini, I., Cantini, F., Katsari, E., and Rosato, A. (2004) Solution structure of the apo and copper(I)-loaded human metallochaperone HAH1. *Biochemistry 43*, 13046–13053.
29. Cornell, W. D., Cieplak, P., Bayly, C. I., Gould, I. R., Merz, K. M., Ferguson, D. M., Spellmeyer, D. C., Fox, T., Caldwell, J. W., and Kollman, P. A. (1995) A Second Generation Force Field for the Simulation of Proteins, Nucleic Acids, and Organic Molecules. *J. Am. Chem. Soc. 117*, 5179–5197.
30. Pearlman, D. A., Case, D. A., Caldwell, J. W., Ross, W. S., Cheatham, T. E., III., DeBolt, S., Ferguson, D., Seibel, G., and Kollman, P. (1995) AMBER, a package of computer programs for applying molecular mechanics, normal mode analysis, molecular dynamics and free energy calculations to simulate the structural and energetic properties of molecules. *Comput. Phys. Commun. 91*, 1–41.
31. Case, D. A., Cheatham, T. E., III., Darden, T., Gohlke, H., Luo, R., Merz, K. M., Jr., Onufriev, A., Simmerling, C., Wang, B., and Woods, R. J. (2005) The Amber biomolecular simulation programs. *J. Comput. Chem. 26*, 1668–1688.
32. Case, D. A., Darden, T. A., Cheatham, T. E., III., Simmerling, C. L., Wang, J., Duke, R. E., Luo, R., Merz, K. M., Pearlman, D. A., Crowley, M., Walker, R. C., Zhang, W., Wang, B., Hayik, S., Roitberg, A., Seabra, G., Wong, K. F., Paesani, F., Wu, X., Brozell, S., Tsui, V., Gohlke, H., Yang, L., Tan, C., Mongan, J., Hornak, V., Cui, G., Beroza, P., Mathews, D. H., Schafmeister, C., Ross, W. S., and Kollman, P. A. (2006) AMBER 9, University of California, San Francisco.
33. Jorgensen, W. L., Chandrasekhar, J., Madura, J., Impey, R. W., and Klein, M. L. (1983) Comparison of simple potential functions for simulating liquid water. *J. Chem. Phys. 79*, 926–935.
34. Hornak, V., Abel, R., Okur, A., Strockbine, B., Roitberg, A., and Simmerling, C. (2006) Comparison of multiple Amber force fields and development of improved protein backbone parameters. *Proteins 65*, 712–725.
35. Berendsen, H. J., Postma, J. P., van Gunsteren, W. F., Di Nola, A., and Haak, J. R. (1984) Molecular dynamics with coupling to an external bath. *J. Chem. Phys. 81*, 3684–3690.

36. Ryckaert, J. P., Ciccotti, G., and Berendsen, H. J. C. (1977) Numerical-integration of Cartesian equations of motion of a system with constraints: Molecular dynamics of N-alkanes. *J. Comput. Phys. 23*, 327–341.
37. Ichiye, T., and Karplus, M. (1991) Collective motions in proteins: A covariance analysis of atomic fluctuations in molecular dynamics and normal mode simulations. *Proteins 11*, 205–217.
38. Rod, T. H., Radkiewicz, J. L., and Brooks, C. L., III. (2003) Correlated motion and the effect of distal mutations in dihydrofolate reductase. *Proc. Natl. Acad. Sci. U.S.A. 100*, 6980 6985.
39. Banci, L., Bertini, I., Cantini, F., Felli, I. C., Gonnelli, L., Hadjiliadis, N., Pierattelli, R., Rosato, A., and Voulgaris, P. (2006) The Atx1-Ccc2 complex is a metal-mediated protein-protein interaction. *Nat. Chem. Biol. 2*, 367–368.
40. Arnold, G. E., and Ornstein, R. L. (1997) Molecular dynamics study of time-correlated protein domain motions and molecular flexibility: Cytochrome P450BM-3. *Biophys. J. 73*, 1147–1159.
41. Hussain, F., Olson, J. S., and Wittung-Stafshede, P. (2008) Conserved residues modulate copper release in human copper chaperone Atox1. *Proc. Natl. Acad. Sci. U.S.A. 105*, 11158–11163.

BI8018652